Phenol methylation on acid catalysts: Study of the catalyst deactivation kinetics and mechanism

M.E. Sad, C.L. Padró, C.R. Apesteguía *

Catalysis Science and Engineering Research Group (GICIC), Instituto de Investigaciones en Catálisis y Petroquímica—INCAPE-(UNL-CONICET), Santiago del Estero 2654, Santa Fe 3000, Argentina

A B S T R A C T

The kinetics and mechanism of coke formation and catalyst deactivation during the synthesis of cresols from phenol methylation were investigated on SiO_2–Al_2O_3, tungstophosphoric acid (HPA) supported on silica, and zeolites HBEA, HZSM5, HMCM22 and HY. The nature, density and strength of surface acid sites were probed by temperature programmed desorption of NH_3 coupled with infrared spectra of adsorbed pyridine. Coke formed on the catalysts during reaction was characterized by temperature programmed oxidation. All the samples deactivated on stream. A linear correlation was observed between the initial catalyst deactivation and the amount of coke, thereby indicating that coke formation was responsible for the activity decay. Coking kinetic studies showed that a significant part of coke was rapidly formed from the reactants. When methanol was feeding alone, significant amounts of carbon were formed on the catalysts (between 0.6% and 6.2%C), particularly on samples containing mainly strong Brønsted acid sites. Nevertheless, the coke amounts formed during phenol methylation were clearly higher (between 3.7% and 14.9%C), which showed that phenol was also responsible for coke formation. More insight on the role of phenol and methanol on coke formation was obtained by characterizing the coke nature using infrared spectroscopy. Coked samples recovered after methanol decomposition reaction exhibited IR absorption bands characteristics of olefinic species formed on Brønsted and Lewis acid sites. The IR spectra of coked samples recovered after phenol methylation showed the presence of phenolate, aromatic and polyaromatic species adsorbed mainly on Lewis acid sites.

© 2014 Elsevier B.V. All rights reserved.

1. Introduction

Cresol isomers are useful intermediates for the synthesis of antioxidants, pharmaceuticals, herbicides, agrochemicals and dyes. *o*-Cresol is commercially produced by gas-phase alkylation of phenol with methanol on solid bases at temperatures between 673 K and 773 K [1–3]. *p*-Cresol is obtained by toluene dehydration via sulfonation with sulphuric acid in a four reaction step process while *m*-cresol is produced by alkaline chlorotoluene hydrolysis or cymene hydroperoxide cleavage [4]. The current syntheses of *m*- and *p*-cresol entail concerns related to corrosion, and disposal of spent and waste materials, and there is therefore a clear interest for developing more ecofriendly synthesis routes, in particular using solid catalysts. In this regard, the alkylation of phenol with methanol has been widely studied at atmospheric pressure on acid catalysts for producing cresols [5–9]. Reports showed that on acid zeolites, silica–alumina or Nafion–H, phenol converts to anisole,

cresols, xylenols and methylanisoles at relatively low temperatures (473–523 K), but the product distribution greatly depend on the nature and strength of surface acid sites and on the catalyst pore microstructure. However, the catalysts suffer from strong deactivation on stream as occurs in similar alkylation reactions [10–12], and thus the potential use of solid acids for obtaining cresol isomers via phenol methylation is hampered because of the rapid activity decay. In spite of that, no studies have been reported yet dealing specifically with the deactivation of solid acids employed for the phenol methylation reaction. In particular, our understanding of the deactivation kinetics and mechanism under reaction conditions is lacking.

In previous works, we studied the synthesis of cresol isomers via the alkylation of phenol with methanol using acid catalysts [13–15]. Research efforts were devoted to elucidate the exact requirements of density, nature and strength of surface acid sites for selectively improving the reaction pathways leading from phenol to a desired cresol isomer.

In particular, we investigated the selective synthesis of *p*-cresol on zeolites HMCM22, HBEA and HZSM5 [14]. We found that the particular pore structure of zeolite HMCM22 promotes by shape selectivity the formation of *p*-cresol at the expense of

* Corresponding author. Tel.: +54 3424555279.
 E-mail addresses: capesteg@fiq.unl.edu.ar,
capesteg@gmail.com (C.R. Apesteguía).

anisole and *o*-cresol among the primary products and drastically suppresses the consecutive reactions forming secondary products. Thus, the *p*-cresol yield and the *para-/ortho*-cresol ratio on HMCM22 for 93% phenol conversion were about 58% and 3.4, respectively, the highest values reported up to now for *p*-cresol formation from methylation of phenol. However, the activity decay on HMCM22 during the progress of the reaction was considerable, thereby suggesting that the reactions forming coke intermediates were not suppressed to any significant extent. In basis of this observation, we decided to extend our studies for the phenol methylation reaction focusing specifically on catalyst activity decay. Thus, in this paper we study the kinetics and mechanism of coke formation and catalyst deactivation during phenol methylation on samples containing essentially strong Brønsted acid sites (HPA/SiO$_2$) and catalysts containing both Lewis and Brønsted acid sites of either strong (zeolites HZSM5, HBEA, HMCM22 and HY) or moderate (SiO$_2$–Al$_2$O$_3$) strength. The aim was to identify the species responsible for coke formation and to establish the relationship between catalyst deactivation and the nature of surface acid sites.

2. Experimental

2.1. Catalyst preparation

The HY zeolite was prepared by triple ion exchange of a commercial NaY zeolite (UOP-Y 54) with ammonium chloride (Merk, 99.8%) at 353 K and subsequent calcination in air. Zeolite HMCM22 was synthesized according to [16], by using sodium aluminate (Alfa Aesar, Technical Grade), silica (Aerosil Degussa 380), sodium hydroxide (Merck, >99%), hexamethyleneimine (Aldrich, 99%) and deionized water as reagents. The molar composition of the synthesis gel was SiO$_2$/Al$_2$O$_3$ = 30, OH/SiO$_2$ = 0.18, hexamethyleneimine/SiO$_2$ = 0.35 and H$_2$O/SiO$_2$ = 45. The gel was transferred to a Teflon lined stainless steel autoclave, rotated at 50 rpm, and heated to 423 K in an oven for 7–10 days. Commercial samples were zeolite HBEA (Zeocat PB), zeolite HZSM5 (Zeocat Pentasil PZ-2/54) and SiO$_2$–Al$_2$O$_3$ (Ketjen LA-LPV). HPA (28%)/SiO$_2$ was obtained by wet impregnation. A suspension of SiO$_2$ powder (Grace G62, 99.7%; 230 m^2/g) was stirred in an aqueous solution of HPA (H$_3$PW$_{12}$O$_{40}$.6H$_2$O, Merck P.A) at room temperature for 24 h. Before reaction, all the samples were treated in air (60 cm^3/min) at 723 K during 3 h, except HPA/SiO$_2$ that was treated at 573 K for 2 h.

2.2. Catalyst characterization

The crystal structure of the samples was determined by powder X-ray diffraction methods (XRD) using a Shimadzu XD-D1 diffractometer and Ni-filtered Cu*K*α radiation. Surface areas were measured by N$_2$ physisorption at its normal boiling point using the BET method in an Autosorb Quantochrome Instrument 1-C sorptometer. The chemical compositions were measured by atomic absorption spectroscopy.

The density and strength of acid sites were determined by temperature-programmed desorption (TPD) of NH$_3$ preadsorbed at 373 K. Samples (100 mg) were treated at 723 K for 2 h in He (60 cm^3/min) and then exposed to a 1% NH$_3$/He stream for 40 min at 373 K. Weakly adsorbed NH$_3$ was removed by flushing with He at 373 K (2 h). The temperature was then increased at 10 K/min and the NH$_3$ concentration in the effluent was measured by mass spectrometry in a Baltzers Omnistar unit.

The nature of surface acid sites of fresh and coked catalysts was determined by infrared spectroscopy (IR) using pyridine as probe molecule and a Shimadzu FTIR Prestige-21 spectrophotometer according to the procedure detailed elsewhere [14]. Fresh

sample wafers were initially outgassed in vacuum at 723 K during 2 h and then a background spectrum was recorded after cooled down to room temperature. Coked sample wafers were outgassed 2 h at 473 K. Spectra were recorded at room temperature, after admission of pyridine, adsorption at room temperature and sequential evacuation at 298 K, 423 K, 573 K, and 723 K.

Coke formed on the catalysts during reaction was measured by temperature programmed oxidation (TPO). Samples (20–100 mg) were heated in a 2% O$_2$/N$_2$ stream from room temperature to 1073 K at 10 K/min. The evolved CO$_2$ was converted into methane passing through a methanation catalyst (Ni/kieselghur) at 673 K. Methane was detected and quantified in a SRI 8610C gas cromatograph equipped with a flame ionization detector.

2.3. Catalyst testing

The gas phase alkylation of phenol (Merck, >99%) with methanol (Merck, 99.8%) was carried out in a fixed bed tubular reactor at 473 K and 101.3 kPa in continuous flow of N$_2$. Samples (0.025–0.6 g, particles with 0.35–0.42 mm diameter) were pretreated in-situ, at 723 K in air flow (75 ml/min) for 2 h before reaction. Methanol (M) and phenol (P) were fed (M/P = 2:1 molar) using a syringe pump and vaporized into flowing N$_2$ to give a N$_2$/(P + M) molar ratio of 26.8. Catalytic runs were carried out at different contact times (W/F_P^0), between 5.6 g h/mol and 560 g h/mol. Samples were collected every 20 min during 4 h and the exit gases were analyzed on-line using an Agilent 6850 gas chromatograph equipped with a flame ionization detector and a 30 m Innowax column (inner diameter: 0.32 mm, film thickness: 0.5 μm). After reaction, catalysts were kept in N$_2$ flow at 473 K during 45 min to desorb reactants and products weakly adsorbed. Phenol conversion (X_P) and methanol conversion (X_M) were calculated as: $X_{P,M} = (Y_{P,M}^0 - Y_{P,M})/Y_{P,M}^0$ a where Y_P^0 and Y_M^0 are the molar fraction of phenol and methanol at the entrance of the reactor while Y_P and Y_M are the molar fraction of phenol and methanol at the exit. The selectivity to product *i* formed from phenol molecules (S_i, mol of product *i*/mol of phenol reacted) was determined as: $S_i = [Y_i/\Sigma Y_i]$ where Y_i is the molar fraction of products formed from phenol.

3. Results and discussion
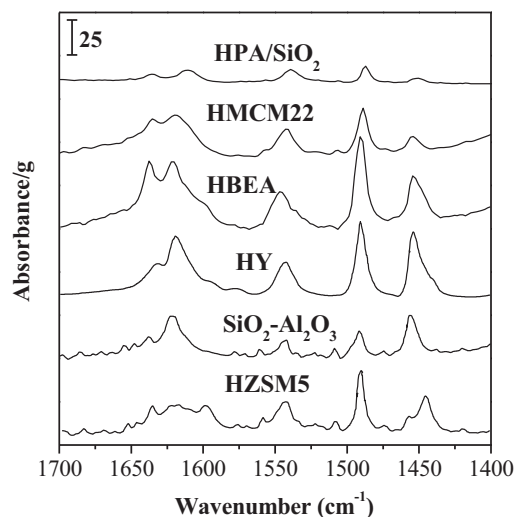
3.1. Catalyst characterization

The chemical composition and surface areas of the samples used in this work are shown in Table 1. Zeolite HY presented the highest S_{BET} value (660 m^2/g) followed by HBEA (560 m^2/g) and SiO$_2$–Al$_2$O$_3$ (540 m^2/g) samples. In the case of HPA/SiO$_2$ the addition of bulky HPA molecules caused only a slight diminution of the SiO$_2$ surface area, from 230 m^2/g to 205 m^2/g. The crystalline structure of zeolite HMCM22 synthesized in our laboratory was checked by XRD technique and the positions and intensities of the diffraction peaks were in good agreement with the HMCM22 diffractograms reported in literature [17].

The sample acid properties (nature, density and strength of acid sites) determined by TPD of NH$_3$ and FTIR of adsorbed pyridine are also presented in Table 1. The total amount of desorbed NH$_3$ was measured by integration of the NH$_3$ TPD curves (not shown here) and it was taken as an indication of the total acid site density. Data in Table 1 show that zeolite HY presented the highest surface acid density on a weight basis (1380 μmol/g) whereas on an areal basis zeolites HZSM5 (2.2 mmol/m^2) and HY (2.1 mmol/m^2) exhibited the highest acid density followed by SiO$_2$–Al$_2$O$_3$ (1.8 mmol/m^2).

The nature and strength of surface acid sites were determined from the FTIR spectra obtained after admission of pyridine at room temperature and sequential evacuation at 423 K, 573 K, and

Table 1
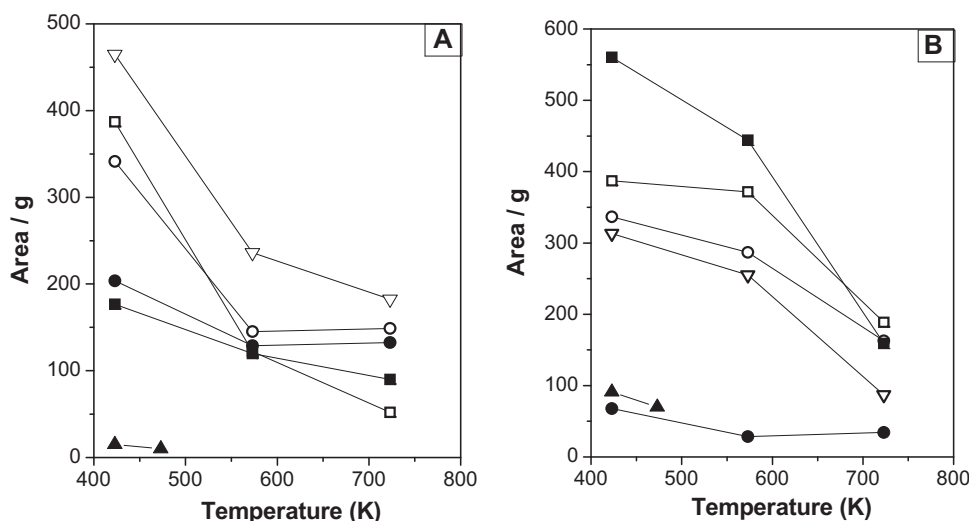Physicochemical and acid properties of the samples.

Sample	Si/Al	HPA (wt%)	Na (wt%)	S_{BET} (m^2/g)	Pore size (Å)	TPD of NH$_3$		FTIR of pyridine[a]		
								Brønsted sites (B)	Lewis sites (L)	L/B
						(µmol/g)	(µmol/m^2)	(area/g)	(area/g)	
HBEA	25.0	–	0.03	560	6.6 × 6.7; 5.6 × 5.6	500	0.9	387	309	0.8
HZSM5	20.0	–	0.43	350	5.1 × 5.5; 5.3 × 5.6	770	2.2	337	341	1.0
HY	2.4	–	0.33	660	7.4 × 7.4	1380	2.1	310	465	1.5
HMCM22	15.0	–	–	400	4.0 × 5.5; 4.1 × 5.1	470	1.2	560	176	0.3
SiO$_2$-Al$_2$O$_3$	11.3	–	–	540	45	1030	1.8	68	204	3.0
HPA/SiO$_2$	–	28	–	205	225	160	0.8	91	15	0.2

[a] FTIR spectra obtained after adsorption of pyridine at 298 K and evacuation at 423 K (B: Brønsted sites; L: Lewis sites).

Fig. 1. FTIR spectra obtained after pyridine adsorption at 298 K and sample evacuation at 423 K.

723 K. FTIR spectra after pyridine adsorption at 298 K and evacuation at 423 K are displayed in Fig. 1. The absorption bands at around 1540 cm^{-1} and between 1440 cm^{-1} and 1460 cm^{-1} arise from pyridine adsorbed on Brønsted and Lewis acid sites, respectively [18–21]. The relative contribution of Lewis and Brønsted acid sites after evacuation of pyridine at 423 K was obtained then by integration of the bands at 1445–1460 cm^{-1} (Lewis) and 1540 cm^{-1} (Brønsted); results are presented in Table 1. The SiO$_2$–Al$_2$O$_3$

sample showed the highest proportion of Lewis sites (L/B = 3). The L/B ratios on zeolites HY, HZSM5 and HBEA were 1.5, 1.0 and 0.8, respectively. Zeolite HMCM22 exhibited mainly Brønsted acidity (L/B = 0.3) which is consistent with previous work reporting L/B ratios between 0.2 and 0.5 for zeolites HMCM22 with Si/Al atomic ratios of about 15 [22,23]. The L/B ratio on HPA/SiO$_2$ was 0.2. The presence of pyridine adsorbed on Lewis acid sites of HPA/SiO$_2$ suggests that upon impregnation of HPA on SiO$_2$, the heteropolyacid partially transforms giving rise to lacunary or unsaturated species of Lewis acid character formed by interaction with the silica support [24].

Fig. 2 shows the evolution of the amount of pyridine adsorbed on surface Lewis and Brønsted sites as a function of the evacuation temperature and gives insight on the acid site strength. Significant amounts of pyridine remained adsorbed on HMCM22, HZSM5 and HY after evacuation at 723 K thereby showing that these zeolites contain strong acid sites. The L/B ratio on HY increased with the evacuation temperature from 1.5 (423 K) to 2.1 (723 K) and probably reflects the fact that a part of the Brønsted sites corresponding to the bridged hydroxyl groups of the structure are of medium strength [25]. The very strong Lewis sites of zeolite HY have been associated with aluminium atoms that are either extra-framework (tetracoordinated) or associated with framework defects (tricoordinated) [25]. In contrast to zeolite HY, the L/B ratio on zeolite HZSM5 did not vary significantly by increasing the desorption temperature. In fact, after degassing at 423 K and 723 K the L/B ratio were 1.0 and 0.9, respectively. In the case of zeolite HMCM22, the L/B ratio increased from 0.3 to 0.5 when the evacuation temperature was increased from 423 K to 723 K. The L/B ratio determined on HBEA evacuated at 423 K (L/B = 0.8) diminished to 0.3 upon

Fig. 2. Lewis (A) and Brønsted (B) peak areas as a function of the evacuation temperature. HY (▽), HBEA (□), HZSM5 (○), SiO$_2$–Al$_2$O$_3$ (●), HMCM22 (■), HPA/SiO$_2$ (▲).
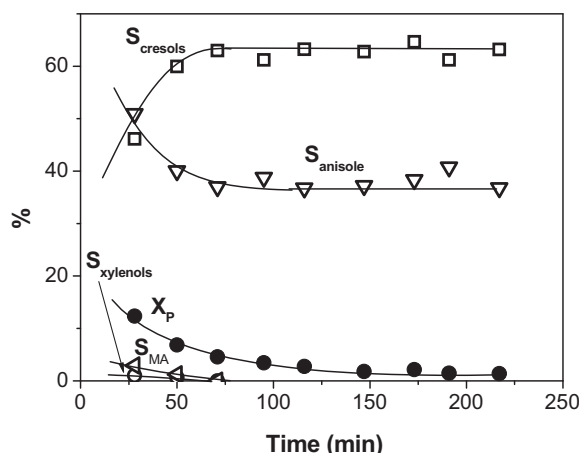
Fig. 3. Phenol conversion (X_P) and selectivities as a function of time-on-stream on HPA/SiO$_2$ [473 K, P_T = 101.3 kPa, W/F_P^0 = 112 g h/mol, P_P = 0.96 kPa, P_M = 1.92 kPa].

evacuation at 723 K. The L/B ratio on SiO$_2$–Al$_2$O$_3$ evacuated at 423 K was 3 (Table 1) and increased to about 4 when the evacuation temperature was increased to 723 K. Finally, after evacuation at 423 K and 473 K, HPA/SiO$_2$ contained almost exclusively Brønsted sites. Overall, the results in Table 1 and Figs. 1 and 2 show that the samples used in this work have different acid properties; i.e. different acid site density, nature and strength.

3.2. Catalytic tests

3.2.1. Phenol methylation: activity and product distribution

Main products in the alkylation of phenol with methanol were cresols, anisole, xylenols and methylanisoles (MA). Dimethylether (DME) and some light hydrocarbons were also formed by dehydration and further condensation of methanol on acid sites. Fig. 3 shows the evolution of phenol conversion (X_P) and selectivities (S_i) as a function of time obtained at 473 K on HPA/SiO$_2$ and typically illustrates the time-on-stream behavior of the catalysts for phenol methylation. Results obtained in previous works [13,14] allowed us to propose the reaction network of Fig. 4 for the methylation of phenol on solid acids. Phenol initially reacts with methanol via two parallel alkylation reactions: by *O*-alkylation phenol is transformed to anisole and by *C*-alkylation yields directly *o*- and *p*-cresols.
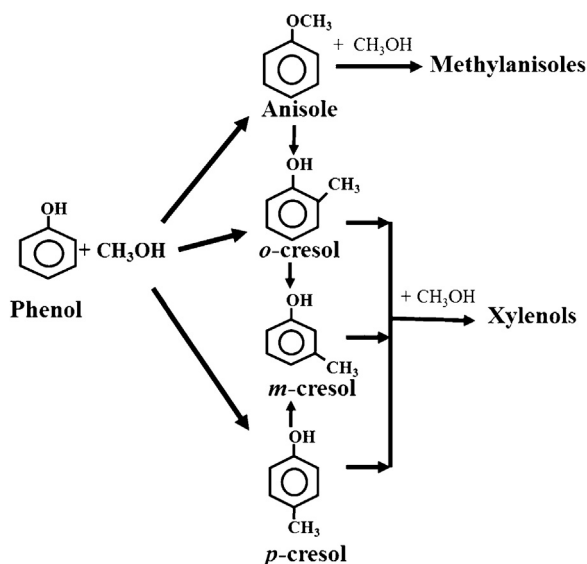

Fig. 4. Reaction network for methylation of phenol on solid acids.

Anisole may in turn produce *o*- and *p*-cresol by alkylating phenol. *m*-Cresol is formed by consecutive isomerization of *o*- and *p*-cresol isomers. Alkylation of *o*- and *p*-cresol isomers with methanol forms 2,4 and 2,6 xylenols, while anisole may reacts with methanol to produce methylanisoles.

Fig. 3 shows that phenol conversion diminished with time-on-stream, reflecting the in-situ sample deactivation. Similar catalyst activity decay was observed on all the samples. Due to catalyst deactivation, initial catalytic results were obtained by extrapolation of reactant and product concentration curves to zero time-on-stream. The phenol conversions obtained at zero time and after 3 h on stream for all the samples are shown in Table 2. Zeolites HBEA and HY showed the highest initial phenol conversions which is consistent with previous work reporting that the formation of cresols by phenol methylation is better promoted on wide pore zeolites containing strong surface Lewis and Brønsted acid sites [13]. Zeolites HZSM5 and HMCM22 presented similar activity ($X_P \cong 35\%$) but were clearly less active than HBEA or HY, in spite of their strong acidity. As proposed elsewhere [14], the phenol methylation rate is probably controlled by intracrystalline diffusion on HZSM5 and HMCM22 taking into account that these two zeolites present the smallest pore sizes (Table 1). HPA/SiO$_2$ showed the lowest initial activity (X_P = 20%) suggesting that phenol methylation is not efficiently promoted on catalysts containing essentially Brønsted acid sites. Methanol conversion was higher than phenol conversion for all the catalysts because methanol was involved in additional parallel reactions forming dimethyleter and hydrocarbons. Nevertheless, methanol was always present among reaction products indicating that the reaction was not limited by total methanol consumption.

The product selectivities obtained at X_P = 20% are also reported in Table 2. On all the catalysts, primary monoalkylated products (anisole and cresols) accounted for more than 85% of total selectivity; minor amounts of secondary dialkylated products (xylenols and methylanisoles) were also obtained. The cresol selectivity on HBEA, HZSM5, HY and SiO$_2$–Al$_2$O$_3$ was about 54%, being *o*-cresol isomer formed in major proportion. In contrast, anisole was the main product on HPA/SiO$_2$ ($S_{anisole}$ = 65%) suggesting that catalysts exhibiting essentially Brønsted acidity will preferentially promote the *O*-alkylation of phenol. The cresol selectivity on HMCM22 was about 90%; the narrow channels of this zeolite completely suppressed the formation of secondary dialkylated compounds. In general, xylenol formation was favored on wide pore zeolites containing strong surface Lewis and Brønsted acid sites (zeolites HBEA and HY) while the selectivity to methylanisoles was lower than 4% on all the samples.

3.2.2. Catalyst deactivation and coke formation

All the catalysts deactivated during the alkylation of phenol with methanol. In Fig. 5 we observe the evolution of the activity (a_P) as a function of time for all the catalysts obtained at similar initial phenol conversions (25–35%); a_P is defined as $a_P = r_P/r_P^0$, where r_P^0 and r_P are the rates of phenol conversion at $t = 0$ and $t = t$, respectively. From the initial slopes of curves a_P vs. t in Fig. 5 we determined the parameter $d_0 = -[da_P/dt]_{t=0}$ that accounts for the initial catalyst deactivation [26]; the obtained d_0 values are included in Table 3. The highest d_0 value (27.0×10^{-3} min^{-1}) was determined on zeolite HY while the lowest initial deactivation was observed for SiO$_2$–Al$_2$O$_3$ ($d_0 = 2.1 \times 10^{-3}$ min^{-1}). HPA/SiO$_2$ and HMCM22 presented similar d_0 values of about 18×10^{-3} min^{-1} that were higher than those corresponding to HZSM5 (14.6×10^{-3} min^{-1}) and HBEA (10.5×10^{-3} min^{-1}).

The catalyst deactivation observed in Fig. 5 could be caused by coke formation from parallel/consecutive reactions of reactants/products on surface active sites. We characterized then the carbonaceous deposits of samples recovered from the catalytic

Table 2
Catalytic results for the alkylation of phenol with methanol.

Catalyst	Phenol conversión[a] X_P (%)		Methanol conversión[a] X_M (%)		Selectivity (X_P = 20%, t = 0)[b] S_i (%)			
	t = 0 h	t = 3 h	t = 0 h	t = 3 h	Anisole	Cresols	Xylenols	MA
HBEA	85	32.0	88	70	33	53	11.5	2.5
HZSM5	35	7.0	75	50	41	54	3	2
HY	73	0.3	80	72	31	54	13	2
HMCM22	34	6.0	83	70	8.5	90	0.5	1
HPA/SiO$_2$	20	2.0	82	65	65	32	0.5	2.5
SiO$_2$–Al$_2$O$_3$	30	17.5	55	50	34	54	9	3

[a] [473 K, P_T = 101.3 kPa, P_P = 0.96 kPa, P_M = 1.92 kPa, W/F_P^0 = 112 g h/mol].
[b] [473 K, P_T = 101.3 kPa, P_P = 0.96 kPa, P_M = 1.92 kPa].
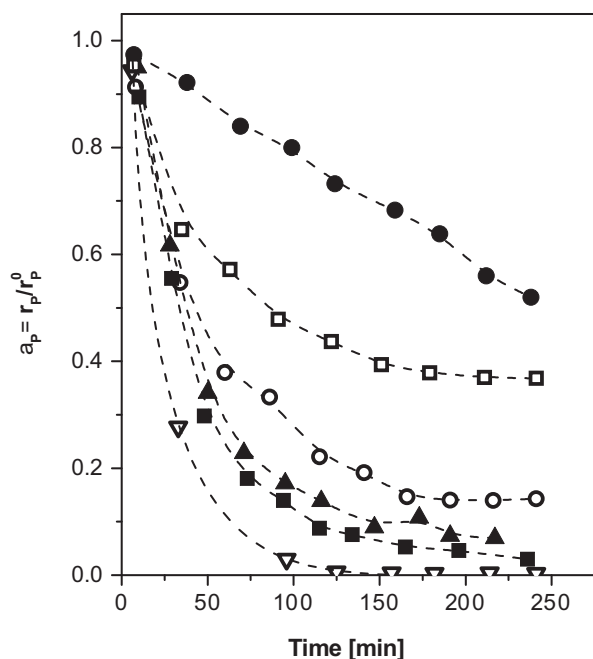

Fig. 5. Activity decay for phenol conversion (a_P) as a function of time on stream. Initial phenol conversions between 25% and 35% [473 K, P_T = 101.3 kPa, P_P = 0.96 kPa, P_M = 1.92 kPa]. SiO$_2$–Al$_2$O$_3$ (●), HBEA (□), HZSM5 (○), HPA/SiO$_2$ (▲), HMCM22 (■), HY (▽)

runs showed in Fig. 5 by performing TPO experiments. Prior the TPO characterization, samples were treated at 473 K in N$_2$ during 45 min. The TPO profiles are presented in Fig. 6. The HPA/SiO$_2$ sample, containing almost exclusively strong Brønsted acid sites, presented a single oxidation peak with a maximum at around 790 K. The TPO curve for HMCM22 exhibited a low-temperature peak at 590 K and a broad combustion band between 600 K and 1030 K. The low-temperature peak probably arises from carbon deposits with high H/C ratio retained in the small channels of this zeolite. HBEA and SiO$_2$–Al$_2$O$_3$ showed a broad combustion band that begins at 600–620 K and ends at about 1050 K. Finally, the TPO profiles for

Table 3
Phenol methylation: initial deactivation d_0 and coke formed after 4 h reaction time.

Catalyst	$d_0 \times 10^3$ (min^{-1})	(%) Carbon	n_C^{as} (mol C/mol acid site)
HBEA	10.5	9.5	15.8
HZSM5	14.6	6.2	14.2
HY	27.0	13.2	7.9
HMCM22	18.8	14.9	26.5
HPA/SiO$_2$	17.5	3.7	19.3
SiO$_2$–Al$_2$O$_3$	2.1	6.0	4.8

[473 K, P_T = 101.3 kPa, P_P = 0.96 kPa, P_M = 1.92 kPa, X_P = 25–35%].

HY and HZSM5 exhibited two superimposed bands at 690–750 K and 880–920 K, respectively.

The amounts of carbon were calculated from the areas under the TPO curves of Fig. 6 and are reported in Table 3 as % Carbon. Significant coke amounts were formed on the catalysts, between 3.7% (HPA/SiO$_2$) and 14.9% (HMCM22). In Table 3 we also included the values of n_C^{as}, number of moles of C deposited per mol of acid sites (acid site density data obtained from TPD of NH$_3$). The highest n_C^{as} values were obtained on HMCM22 (n_C^{as} = 26.5) and HPA/SiO$_2$ (n_C^{as} =19.3), probably due to the predominant presence of strong Brønsted acid sites on both samples. HBEA and HZSM5 that contain L/B acid site ratios of about 1 (Table 1) formed similar amounts of C per acid site (n_C^{as} between 14 and 16). The lowest n_C^{as} value was determined on SiO$_2$–Al$_2$O$_3$ (n_C^{as} =4.8), probably reflecting its moderate acid strength.

In order to get more insight on the relationship between catalyst deactivation and coke formation, we plotted in Fig. 7 initial deactivation d_0 as a function of n_C^{as} for samples recovered from the reactor after performing catalytic tests for 40 min and 4 h. A linear correlation between d_0 and n_C^{as} was obtained for all the catalysts (excepting HY) in both cases, thereby suggesting that coke formation is responsible for the activity decay observed in Fig. 5 by blocking the surface active sites required for the reaction to proceed. The different deactivation behavior observed for zeolite HY is consistent with previous work showing that the activity decay is usually higher on HY than on HZSM5 or HBEA [27]. This is probably due to fact that zeolite HY contains large cages only accessible
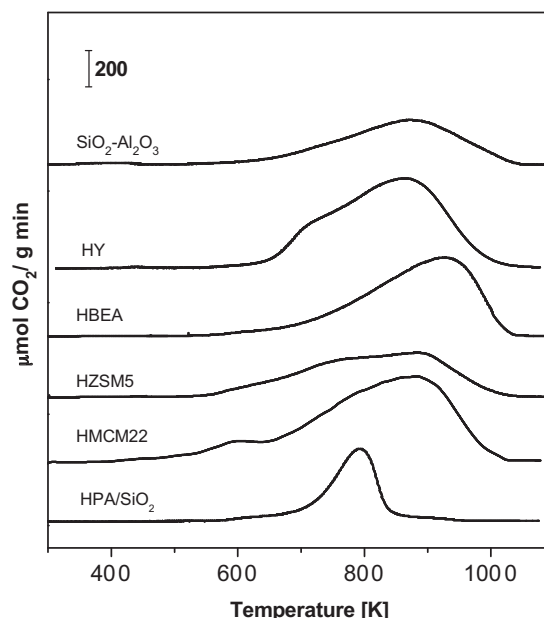

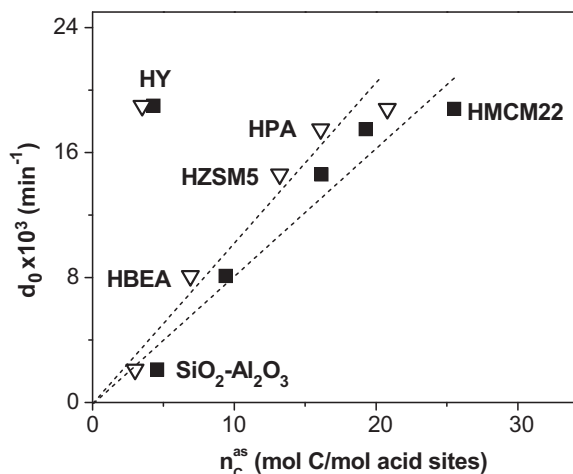**Fig. 6.** TPO profiles of samples recovered from the catalytic runs showed in Fig. 5.

Fig. 9. TPO profiles of HBEA samples recovered after using in 4-h phenol methylation runs at different contact times: (a) 56 g h/mol phenol, (b) 112 g h/mol phenol and (c) 168 g h/mol phenol [473 K, P_T = 101.3 kPa, P_P = 0.96 kPa, P_M = 1.92 kPa].

through small pores. Coke easily formed in large cages produces then severe stereochemical blockage and pronounced deactivation [28].

3.2.3. Catalyst deactivation kinetics and mechanism

Several catalytic runs of different length were performed in order to attain deeper knowledge on the kinetics of coke formation. Specifically, phenol methylation was carried out on zeolite HBEA during 20 min, 40 min and 240 min, and the catalysts recovered from these runs were characterized by TPO experiments as shown in Fig. 8. The TPO profile shapes were qualitatively similar, thereby suggesting that the coke nature did not change significantly with time on stream. The amounts of coke determined by integrating the TPO curves of Fig. 8 were 5.7%, 7.0% and 9.5% after 20 min, 40 min, and 240 min of reaction, respectively. Thus, about 60% of the total coke determined after the 240-min catalytic run was formed during the initial 20 min on stream. Qualitatively, similar coke formation kinetics was obtained on HZSM5, HY, HMCM22
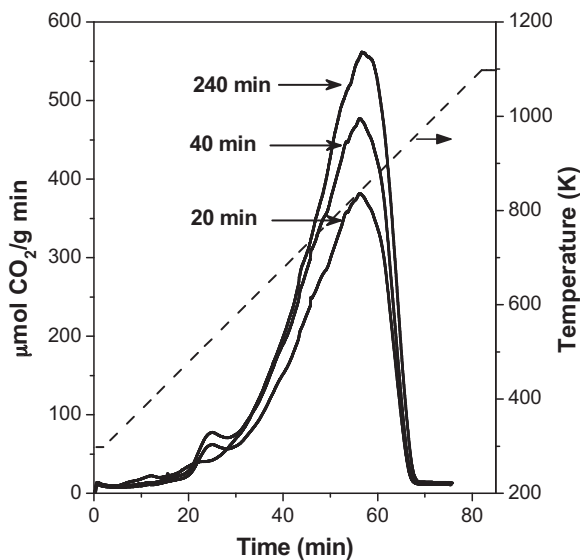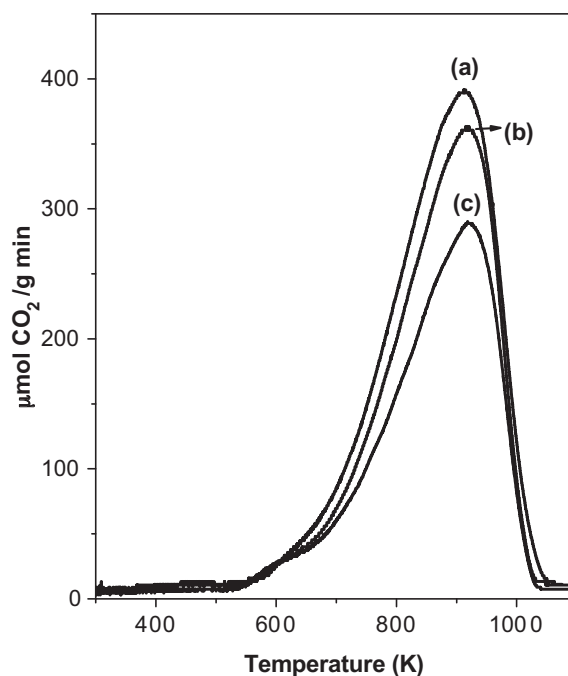
and SiO_2–Al_2O_3 samples (results not shown here), thereby suggesting that a significant part of coke is rapidly formed from reactants.

To obtain more insight on the species responsible for catalyst deactivation, we performed additional catalytic tests on zeolite HBEA at different contact times. In Fig. 9 we compared the TPO profiles of HBEA samples recovered after using in phenol methylation runs of 4-h length at contact times between 56 g h/mol and 168 g h/mol. The TPO profile shapes in Fig. 9 were qualitatively similar but the area under the curves (i.e. the amount of coke) increased
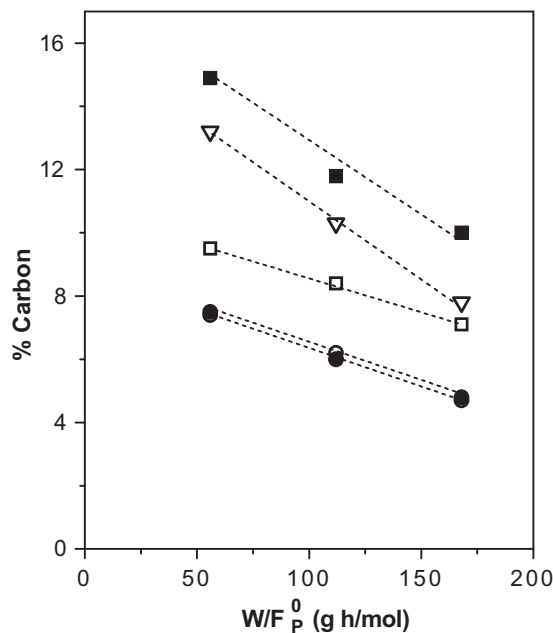

Fig. 7. Initial catalyst deactivation (d_0) versus n_C^{as} (moles of C per mol of acid site). Samples recovered after 40 min (▽) and 4 h (■) on stream for phenol methylation [473 K, P_T = 101.3 kPa, P_P = 0.96 kPa, P_M = 1.92 kPa, W/F_P^0 = 112 g h/mol].

Fig. 8. TPO profiles of HBEA samples recovered after using in phenol methylation runs of 20 min, 40 min and 240 min length [473 K, P_T = 101.3 kPa, P_P = 0.96 kPa, P_M = 1.92 kPa, W/F_P^0 = 112 g h/mol].

Fig. 10. Phenol methylation: Coke formed after 4 h reaction as a function of contact time [473 K, P_T = 101.3 kPa, P_P = 0.96 kPa, P_M = 1.92 kPa]. HMCM22 (■), HY (▽), HBEA (□), HZSM5 (○), SiO_2-Al_2O_3 (●)
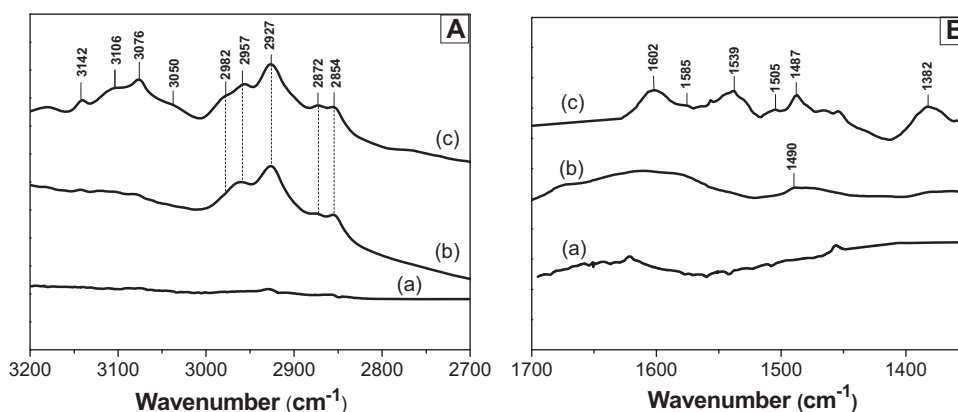
Fig. 11. 2700–3200 cm^{-1} (A) and 1350–1700 cm^{-1} (B) FTIR spectra regions obtained for: (a) fresh HBEA sample; (b) HBEA sample recovered after 4-h methanol decomposition reaction; (c) HBEA sample recovered after 4-h phenol methylation reaction.

when contact time (and phenol conversion) decreased. Actually, the effect of contact time on coke formation was studied on all the catalysts used in this work. In Fig. 10 we have plotted for all the catalysts the % carbon formed after the 4-h catalytic runs as a function of contact time. It is observed that in all the cases the amount of coke increased when contact time was decreased thereby confirming that catalyst deactivation is related with the presence of the reactants, methanol and/or phenol.

Therefore, we decided to study the formation of coke on our catalysts when only methanol is feeding to the reactor at the standard operation conditions used for phenol methylation. We analyzed the methanol decomposition products (DME and hydrocarbons) and determined the carbon amounts formed on the catalysts by TPO technique. Results are shown in Table 4. On all the catalysts, methanol conversion (X_M) was higher than 70% and no noticeable catalyst deactivation was observed during the 4-h reaction time. The highest X_M value was obtained on HPA/SiO$_2$ (96%) that contains essentially strong Brønsted acid sites (Table 1). Zeolites HY, HBEA, HZSM5 and HMCM22 (containing both Brønsted and Lewis acid sites of relatively high strength) were also very active for converting methanol (X_M = 85–90%). Finally, methanol conversion was only 70% on SiO$_2$–Al$_2$O$_3$ that exhibits moderate acid strength. Formation of coke from methanol decomposition on solid acids has been studied by other authors [29–33]. It has been proposed that methanol is initially dehydrated to dimethylether on either Brønsted or Lewis acid sites and then light hydrocarbons such as methane, ethene, ethane, propane, propene, and aromatics may be formed preferentially on Brønsted acid sites [31]. Consistent with this proposal, we observed here that all our catalysts produced DME which suggests that methanol dehydration is promoted on Lewis and Brønsted acid sites indistinctively. Besides, we also observed that hydrocarbon formation was particularly favored on samples containing predominantly strong Brønsted acid sites such as HPA/SiO$_2$, HY or HMCM22.

Table 4
Methanol decomposition reaction: conversion and coke formation.

Catalyst	X_M (%)[a]	(%) Carbon[b]
HBEA	89	3.8
HZSM5	85	3.4
HY	85	5.5
HMCM22	86	5.3
HPA/SiO$_2$	96	1.9
SiO$_2$–Al$_2$O$_3$	70	0.6

[473 K, P_T = 101.3 kPa, P_M = 1.92 kPa, W/F_M^0 = 57.9 g h/mol].
[a] Methanol conversion was constant during the 4-h catalytic tests.
[b] Determined by TPO technique after 4 h reaction.

Although methanol conversion remained constant with time on stream, the catalysts changed their color at the end of the runs suggesting the presence of carbonaceous deposits on the catalyst surface. The amounts of carbon formed on all the samples were determined by TPO technique and the results are given in Table 4. In general, the amount of coke increased with catalyst activity for the methanol decomposition reaction. For example, the highest amount of coke (6.2%) was determined on HPA/SiO$_2$, the most active catalyst, while SiO$_2$–Al$_2$O$_3$ formed only 0.6% carbon. What is important to remark here is that in spite of that methanol decomposition formed significant amounts of coke on the catalysts, the %C values presented in Table 4 were clearly lower than those formed on the corresponding catalysts during phenol methylation (Table 3). These results strongly suggested that phenol is also responsible for coke formation in the alkylation of phenol with methanol, either because of its strong adsorption on surface active sites or because of secondary phenol/methanol reactions producing coke intermediates. To obtain more insight on the role of phenol and methanol in the formation of coke, we performed additional experiences by characterizing the nature of coke using FTIR spectroscopy.

3.2.4. Study of nature of coke by FTIR spectroscopy

We used FTIR spectroscopy to characterize the coke formed on HBEA during phenol methylation and methanol decomposition reactions. Samples were recovered after carrying out both reactions under the same operation conditions for 4 h. Fig. 11 shows the FTIR spectra obtained on fresh and coked HBEA samples in the two most important frequency regions to characterize coke, i.e. 1350–1700 cm^{-1} and 2700–3200 cm^{-1} regions [34]. Coked HBEA sample recovered after methanol decomposition reaction showed in the 2700–3200 cm^{-1} region (Fig. 11A, spectrum b) several bands at 2854 cm^{-1} (–CH$_2$ groups), 2872 cm^{-1} and 2957 cm^{-1} (–CH$_3$ groups), 2927 cm^{-1} (–CH$_2$ and –CH groups) and 2982 cm^{-1} (olefins groups) [35]. This sample also exhibited a very broad absorption band between 1695 cm^{-1} and 1550 cm^{-1} (Fig. 11B, spectrum b) attributed mainly to C–C double bond stretch of olefins [36]. Coked HBEA sample recovered after phenol methylation displayed several IR bands in the 1350–1700 cm^{-1} region (Fig. 11B, spectrum c). The bands at 1505 cm^{-1} and 1487 cm^{-1} are consistent with the presence of adsorbed phenol species [36] whereas the bands at 1602 cm^{-1}, 1585 cm^{-1} and 1539 cm^{-1} are characteristic of C–C stretching vibrations of polyaromatics compounds [35]. The IR band appearing at 1382 cm^{-1} supports the presence of methyl groups linked to aromatic compounds [36]. In the 2700–3200 cm^{-1} region (Fig. 11A, spectrum c), this coked HBEA sample presented all the IR absorption bands associated with carbonaceous species formed from methanol decomposition, and additional bands at
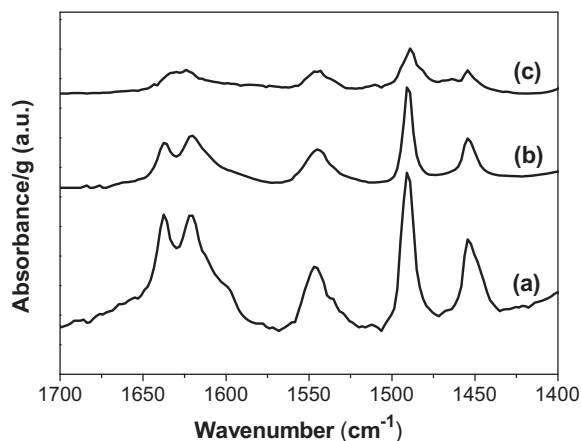
Fig. 12. FTIR spectra of pyridine adsorbed at 298 K and evacuated at 423 K on: (a) fresh HBEA sample; (b) HBEA sample recovered after 4-h methanol decomposition reaction; (c) HBEA sample recovered after 4-h phenol methylation reaction.

$3050\,cm^{-1}$, $3076\,cm^{-1}$, $3106\,cm^{-1}$ attributable to adsorbed phenol, olefinic CH_2 groups, and benzene groups, respectively [34,35]. In summary, IR spectra in Fig. 11 show that methanol decomposition forms carbonaceous olefinic species on the catalyst surface while cofeeding methanol/phenol causes the formation of additional adsorbed phenolate, aromatic and polyaromatic species.

In an attempt to ascertain the relationship between coke formation and the nature of surface acid sites, we characterized the coked HBEA samples of Fig. 11 by FTIR of adsorbed pyridine. Coked HBEA sample wafers were outgassed 2 h at 473 K and then a background spectrum was recorded after cooled down to room temperature. Then pyridine was admitted at room temperature and desorbed at 423 K before recording the IR spectrum. The obtained pyridine IR spectra presented in Fig. 12 are difference spectra where the coked HBEA spectra served as the reference. Spectrum (a) shows the bands characteristics of pyridine absorbed on Lewis ($1450\,cm^{-1}$) and Brønsted sites ($1540\,cm^{-1}$) on fresh HBEA zeolite; the L/B ratio is 0.8 as reported in Table 1. In spectrum (b) corresponding to HBEA sample recovered after 4-h methanol decomposition reaction it is observed that the bands at $1450\,cm^{-1}$ and $1540\,cm^{-1}$ decreased in about the same proportion as compared to those of fresh HBEA sample. In contrast, spectrum (c) shows that the Lewis sites band decreased in higher proportion than that of Brønsted sites on HBEA sample recovered after 4-h phenol methylation reaction. As a consequence, the L/B ratio on this sample diminished to 0.3. This late result is consistent with previous reports showing that phenol is adsorbed preferentially on Lewis acid centers, predominantly in vertical orientation [37,38]. The preferential adsorption of phenol on Lewis acid sites allows us to explain data in Table 2 showing that the phenol conversion decay during the progress of phenol methylation reaction was clearly higher than that of methanol conversion. In fact, the IR spectra of Fig. 11 indicated that part of coke formed on the catalysts are adsorbed phenolate species that would deactivate Lewis acid sites required to promote phenol methylation. In contrast, methanol decomposition may proceed on Brønsted acid sites via dehydration, dehydrogenation and condensation reactions that will be not deactivated by coking on Lewis acid sites.

4. Conclusions

The catalyst activity, selectivity and stability for phenol methylation greatly depend on the surface acid properties. Wide pore zeolites containing strong surface Lewis and Brønsted acid sites such as zeolites HBEA and HY are highly active for this reaction. Zeolites HZSM5 and HMCM22 present also strong acidity, but the

phenol conversion rate on both samples is lower than that on HBEA and HY because the reaction is probably controlled by intracrystalline diffusion. Phenol methylation is not favored on samples that present moderate Lewis and Brønsted acidity (SiO_2–Al_2O_3) or contain only strong Brønsted acid sites (HPA/SiO_2).

All the samples deactivated on stream because of coke formation. The initial catalyst deactivation decreased linearly with the amount of coke, excepting for zeolite HY. The major part of coke is formed rapidly from methanol/phenol reactants and therefore the amount of coke formed on the catalysts decreases with contact time (and phenol conversion). Methanol reactions form significant carbonaceous deposits, particularly on samples containing predominantly strong Brønsted acid sites such as zeolite HMCM22 and HPA/SiO_2. Nevertheless, the coke amount formed in the phenol methylation reaction is significantly higher than that formed on the corresponding catalyst during methanol decomposition showing that phenol is the main responsible for coke formation. Methanol decomposition builds carbonaceous olefinic species on the catalyst surface while cofeeding methanol/phenol forms additional adsorbed phenolate, aromatic and polyaromatic species, mainly on Lewis acid sites. The preferential adsorption of phenol on Lewis acid sites required to promote phenol methylation explains the fact that phenol conversion decay is clearly higher than that of methanol conversion during the progress of this reaction. In fact, methanol decomposition can simultaneously proceed on Brønsted acid sites via parallel dehydration, dehydrogenation and condensation reactions.

References

[1] G.L. Gregory, US Patent 4933509, General Electric Co., 1989.
[2] S. Sato, K. Koizumi, F. Nozaki, Appl. Catal., A 133 (1995) L7–L10.
[3] F. Cavani, L. Maselli, S. Passeri, J.A. Lercher, J. Catal. 269 (2010) 340–350.
[4] Willey-VCH (Ed.), Ullman's Encyclopedia of Industrial Chemistry, seventh ed., Willey-VCH, Wenheim, 2011.
[5] S. Balsama, P. Beltrame, P.L. Beltrame, P. Carniti, L. Forni, G. Zuretti, Appl. Catal. 13 (1984) 161–170.
[6] M. Renaud, P. Chantal, S. Kaliaguine, Can. J. Chem. Eng. 64 (1986) 787–791.
[7] M. Marczewski, G. Perot, M. Guisnet, in: M. Guisnet, J. Barrault, C. Bouchoule, D. Duprez, C. Montassier, G. Pérot (Eds.), Studies in Surface Science and Catalysis, 41, Elsevier, Amsterdam, 1988, p. 273.
[8] M. Marczewski, J.P. Bodibo, G. Perot, M. Guisnet, J. Mol. Catal. 50 (1989) 211–218.
[9] E. Santacesaria, D. Grasso, D. Gelosa, S. Carrá, Appl. Catal. 64 (1990) 83–99.
[10] G. Mirth, J. Cejkab, J.A. Jan Krtilb, Lercher, in: B. Delmon, G.F. Froment (Eds.), Studies in Surface Science and Catalysis, 88, Elsevier, Amsterdam, 1994, p. 241.
[11] M. Han, S. Lin, E. Roduner, Appl. Catal., A 243 (2003) 175–184.
[12] M.N. Vanoy-Villamil, C.R. Apesteguía, C.L. Padró, Microporous Mesoporous Mater. 181 (2013) 54–60.
[13] M.E. Sad, C.L. Padró, C.R. Apesteguía, Catal. Today 133–135 (2008) 720–728.
[14] M.E. Sad, C.L. Padró, C.R. Apesteguía, Appl. Catal., A 342 (2008) 40–48.
[15] M.E. Sad, C.L. Padró, C.R. Apesteguía, J. Mol. Catal. A: Chem. 327 (2010) 63–72.
[16] M.K. Rubin, P. Chu, US Patent 4,954,325, 1990.
[17] S.L. Lawton, A.S. Fung, G.J. Kennedy, L.B. Alemany, C.D. Chang, G.H. Hatzikos, D.N. Lissy, M.K. Rubin, H.K.C. Timken, S. Steuernagel, D.E. Woesner, J. Phys. Chem. 100 (1996) 3788–3798.
[18] E.P. Parry, J. Catal. 2 (1963) 371–379.
[19] J.W. Ward, J. Catal. 10 (1968) 34–46.
[20] H. Knözinger, Adv. Catal. 25 (1976) 184–271.
[21] G. Busca, Catal. Today 41 (1998) 191–200.
[22] D. Meloni, S. Laforge, D. Martin, M. Guisnet, E. Rombi, V. Solinas, Appl. Catal., A 215 (2001) 55–66.
[23] A. Corma, C. Corell, V. Fornés, W. Kolodziejski, J. Pérez-Pariente, Zeolites 15 (1995) 576–582.
[24] V.K. Diez, C.R. Apesteguia, J.I. Di Cosimo, Catal. Lett. 123 (2008) 213–219.
[25] A. Boréave, A. Aroux, C. Guimon, Microporous Mater. 11 (1997) 275–291.
[26] C.L. Padró, C.R. Apesteguía, Catal. Today 107–108 (2005) 258–265.

[27] G. Elordi, M. Olazar, G. Lopez, P. Castaño, J. Bilbao, Appl. Catal., B 102 (2011) 224–231.
[28] H.S. Cerqueira, G. Caeiro, L. Costa, F. Ramôa Ribeiro, J. Mol. Catal. A: Chem. 292 (2008) 1–13.
[29] H. Knözinger, K. Kochloeft, W. Meye, J. Catal. 28 (1973) 69–75.
[30] H. Knözinger, D. Dautzenberg, J. Catal. 3 (1974) 142–144.
[31] T. Tsoncheva, R. Dimitrova, Appl. Catal., A 225 (2002) 101–107.
[32] S.H. Campbell, X.-Z. Jiang, R.F. Howe, Microporous Mesoporous Mater. 29 (1999) 91–108.
[33] V. Vishwanathan, K.-W. Jun, J.-W. Kim, H.-S. Roh, Appl. Catal., A 276 (2004) 251–255.
[34] I. Graca, J.D. Comparot, S. Laforge, P. Magnoux, J.M. Lopes, M.F. Ribeiro, F. Ramoa Ribeiro, Appl. Catal., A 353 (2009) 123–129.
[35] P. Castaño, G. Elordi, M. Olazar, A.T. Aguayo, B. Pawelec, J. Bilbao, Appl. Catal., B 104 (2011) 91–100.
[36] R.T. Conley, Infrared Spectroscopy, second ed., Allyn and Bacon, Boston, MA, 1972.
[37] K.V.R. Chary, K. Ramesh, G. Vidyasagar, V.V. Rao, J. Mol. Catal. A: Chem. 198 (2003) 195–204.
[38] K. Tanabe, T. Nishizaki, in: G.C. Bond, P.B. Wells, F.C. Tompkins (Eds.), Proceedings of the Sixth International Conference on Catalysis vol. 2, The Chemical Society, London, 1977, p. 863.